

Hundreds of Earthquakes per Day: The 2014 Guthrie, Oklahoma, Earthquake Sequence

by Harley M. Benz, Nicole D. McMahon, Richard C. Aster, Daniel E. McNamara, and David B. Harris

Online Material: Gutenberg–Richter plot, b -values and associated p -values, magnitudes and number of detections per day, and earthquake catalog.

INTRODUCTION

A remarkable increase in seismic activity in Oklahoma since 2009 has been shown to correlate closely with enhanced hydrocarbon extraction and associated wastewater disposal; 99% of this recent Oklahoma earthquake activity has occurred within 15 km of a class II injection well (Ellsworth, 2013). In response to this increase in seismic activity, the U.S. Geological Survey (USGS) partnered with the Oklahoma Geological Survey (OGS) to exchange waveform data from permanent and temporary seismic stations to improve the cataloging of earthquake source parameters for a broad region of north-central Oklahoma. For a particularly persistent earthquake sequence near Guthrie, Oklahoma, a subspace detection method is applied to data from nearby seismic stations. This approach documents the occurrence of hundreds of readily detectable, highly similar, earthquakes per day, with rates occasionally exceeding 1000 earthquakes per day. Time-varying changes in b -value appear episodic, suggesting a correlation with periods of reversible fault weakening and associated failure.

Real-time seismic monitoring typically uses automated transient detection-based pickers to detect earthquakes and to define onset times of seismic phases. Such methods cannot reliably detect earthquake signals or time phases with low signal-to-noise, resulting in less complete earthquake catalogs than may be recovered by other means. Recognizing this limitation, recent studies of a suspected induced-seismicity sequence near Youngstown, Ohio, used waveform template matching (Kim, 2013; Skoumal *et al.*, 2014) to significantly lower the detection threshold and to better characterize the spatiotemporal variability of seismicity. In this article, we build on this effort using subspace detectors to objectively minimize the number of waveform templates required to fully characterize an earthquake sequence while increasing computational efficiency. Results demonstrate a new and scalable real-time procedure to better detect and characterize the rates, locations, magnitudes, and source processes of earthquake sequences of

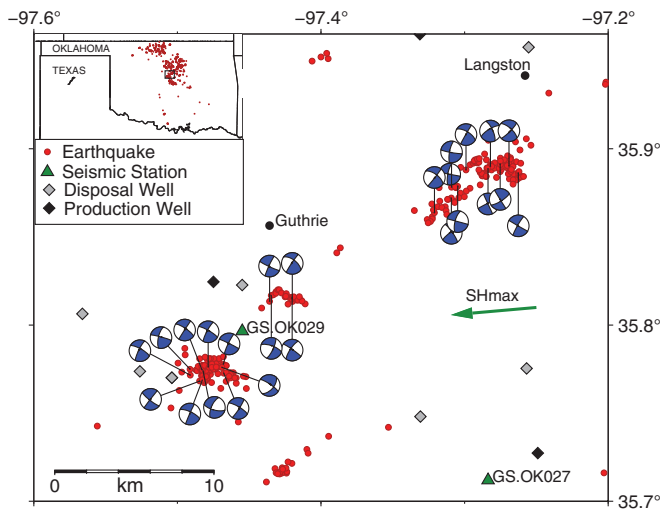
interest to the USGS National Earthquake Information Center (NEIC).

To better monitor and characterize Guthrie earthquake activity, we implemented optimal waveform detectors for a particularly active earthquake sequence, as identified by previously recorded earthquakes. What we found for the Guthrie sequence was extraordinary—hundreds of readily detectable earthquakes per day that continued throughout a seven-month study period. Using a relative amplitude master event method to estimate the magnitudes of these highly similar and nearly collocated earthquakes, temporal changes in b -value can be analyzed; the b -value is a number that describes earthquake frequency–magnitude distribution (FMD) and that provides possible physical insights into the earthquake-generation process. The correlation and detection processing was executed using NEIC acquisition systems and software processing subsystems, thus making it relatively easy to operationalize as a standard real-time procedure and to apply to other seismogenic areas of interest.

SEISMICITY IN THE VICINITY OF GUTHRIE, OKLAHOMA

At the time of this study, the OGS operated 12 permanent broadband and short-period stations within Oklahoma, whereas the USGS and Incorporated Research Institutions for Seismology (IRIS) operated an additional three permanent broadband and strong-motion stations, as well as numerous stations in surrounding states. To augment existing USGS and OGS monitoring capabilities, the USGS and OGS coordinated the deployment of an additional 12 real-time temporary stations that provide additional coverage of fault systems that had recently become active. Two of these temporary stations, GS.OK027 and GS.OK029, were deployed to help monitor seismic activity that emerged in late 2013 and early 2014 near Guthrie and Langston, Oklahoma (Fig. 1).

The USGS earthquake catalog for central Oklahoma was improved using a multiple-event relocation procedure (McNamara *et al.*, 2015). The relocated earthquakes show both well-defined clusters of seismicity and prominent linear trends of seismicity throughout the region (Fig. 1). Source mechanisms



▲ **Figure 1.** Location map of features near the Guthrie, Oklahoma, study site. The red dots show the distribution of earthquakes near Guthrie and Langston, Oklahoma, whereas the green triangles show the two closest seismic stations. The regional moment tensor solutions for the largest earthquakes in the various earthquake sequences and the active class II injection wells in the vicinity (gray and black diamonds) are also shown. The green arrow indicates the direction of maximum horizontal compression at N85° E. The inset map shows the study area within the Oklahoma region and seismicity from February 2014 through August 2014. © Well information is available in Table S2.

of the earthquakes are typically strike slip with fault planes striking either northwest–southeast or northeast–southwest and optimally oriented relative to the N85°E direction of maximum horizontal compression (Holland, 2013; McNamara *et al.*, 2015). The Guthrie cluster southwest of station GS.OK029, centered at approximately 35.77° N and 97.44° W, is notable for generating a large number of earthquakes, including 79 located by the routine operations of the NEIC, with 33 events being *M* 3 or greater, and source depths ranging between 3 and 8 km. The region exhibited sustained seismic activity throughout 2014 within 5 km of two active class II disposal wells (<http://www.occpermit.com/WellBrowse/>; last accessed May 2015). Reported earthquake magnitudes in the cluster range from 2.0 to 4.0, with six earthquakes large enough for the NEIC to determine a regional moment tensor (RMT) solution (Herrmann *et al.*, 2011). All ten RMT solutions are strike-slip mechanisms with one nodal plane aligning with the seismicity that is elongated in the northwest–southeast direction, suggesting earthquakes occurring on a steeply dipping, left-lateral strike-slip fault.

Station GS.OK029 (Fig. 1), which was installed on 15 February 2014, operates with three continuous broadband channels at 100 samples/s and three triggered strong-motion channels at 200 samples/s. This station’s close proximity to the Guthrie cluster (~3.5 km from the cluster’s centroid) makes it ideal for applying the subspace detector method to better characterize the size and the temporal and spatial patterns of the earthquake sequence. Station GS.OK027 (Fig. 1) was installed

on 14 February 2014 and is configured similarly to GS.OK029. Applying the same processing to station GS.OK027 provides independent estimates of the source parameters and enables us to evaluate detector performance as a function of distance from this prolific source region.

PROCESSING METHODS

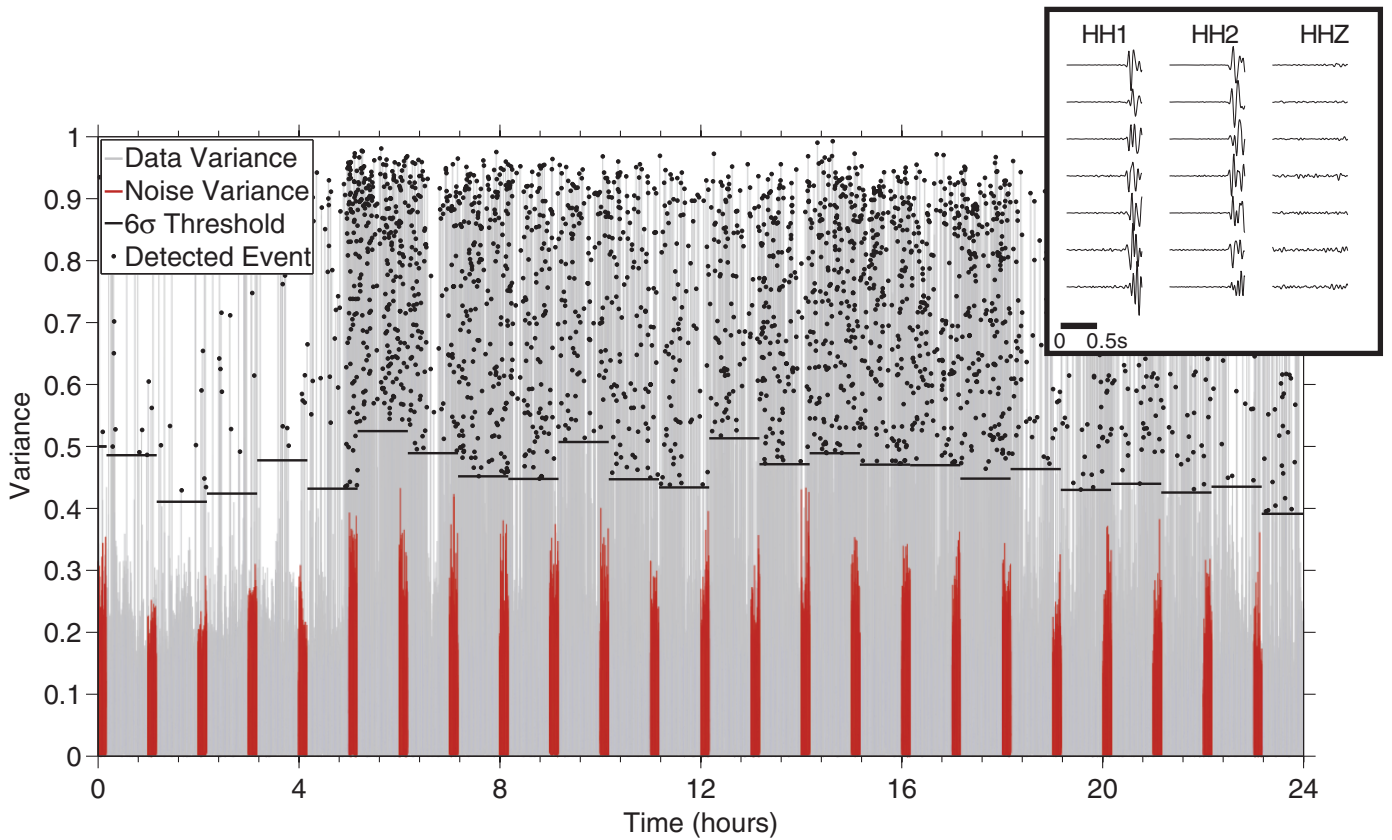
Subspace Detectors

Subspace detection is a powerful and adaptive tool that can improve earthquake catalogs by detecting small amplitude earthquake signals in the presence of noise within continuous data streams. This study closely follows the methodology of Harris (2006) and Harris and Dodge (2011), in which an optimal set of subspace detectors are constructed by the singular value decomposition of a matrix with columns that represent a large set of aligned observed earthquake waveforms (which may be multichannel) previously recorded by a station of interest. The singular value spectrum provides both a direct measure of the similarity of the observed waveforms and a measure of how many orthogonal basis vectors (templates) are needed to adequately represent the observed data to a specified degree. The data space basis vectors associated with the highest-rank singular values become the set of component basis functions of a single multidimensional template that best describes the seismic sequence being evaluated. The number of basis functions (templates) needed to adequately describe seismograms from an earthquake sequence is a function of the variability of the observed waveforms, which is related to changes in source time history, source mechanism, and spatial distribution of the earthquakes.

Correlating the subspace detector templates with the observed data provides a point-by-point measure of the similarity of the detectors to the event space. In the implementation used here, the correlation is a least-squares estimate of the fit of the multidimensional (rank > 1) template (Fig. 2) to the observed data. For a single-rank multichannel template, the fit is equivalent to the square of the correlation coefficient with a range between 0 and 1. Detections are declared for peaks that exceed a specified threshold.

The detection threshold is determined by empirical estimates of noise. In the frequency domain, the spectral amplitude of the observed data is combined with the transformed filtered Gaussian random noise that is substituted for the phase, done on a channel-by-channel basis. The resulting empirical noise template mimics the spectral shape of each template but has randomized phase characteristics. For the Guthrie case, correlation of the empirical noise templates with the observed data shows that the histogram of the results has a Gaussian shape. In this study, detections are declared when the peak in the correlation results exceeds a 6σ threshold, which we judged to be low enough to detect most of the events above the noise floor of the sensor but high enough to minimize false detections.

Based on the similarity of RMT nodal planes and alignment of seismicity, we assume that detections within



▲ **Figure 2.** Station GS.OK029 subspace cross-correlation results for 17 February 2014. The light gray shows the variance of the cross correlation between the templates and continuous three-component data for station GS.OK029, and the red shows the variance using empirical noise templates to estimate the noise floor of the cross correlation. The horizontal black lines indicate the 6σ threshold above which peaks are considered as event detections. The small black circles show the location and value of the detection peaks. (Inset) The template set through rank 7 filtered in the 4–16 Hz frequency band, with the rank decreasing from top to bottom.

the Guthrie sequence will have a similar style of faulting. Consequently, we use the M_w and three-channel waveforms from a previously modeled earthquake (22 May 2014, M_w 3.5) as a reference for computing detection magnitudes. The detection magnitude (M) is determined by

$$M = M_{\text{ref}} + \log_{10} \left(\frac{x \cdot y}{x \cdot x} \right), \quad (1)$$

in which M_{ref} is the magnitude of the reference earthquake, $x \cdot y$ is the dot product of the multichannel waveforms for the reference earthquake (x) and the detected waveforms (y), and $x \cdot x$ is the dot product of the waveforms for the reference earthquake. Using different reference events for which we have a well-determined moment magnitude yields similar results.

Estimate of Time-Varying b -Value

The FMD of a population of earthquakes is commonly and successfully modeled as a power law relationship (Ishimoto and Iida, 1939; Gutenberg and Richter, 1944), such that

$$\log_{10} N = a - bM, \quad (2)$$

in which N is the cumulative number of earthquakes greater than or equal to magnitude M , and a and b are constants describing the activity and slope, respectively. The constant b , for a specific event population, characterizes the relative frequency of occurrence for different size events; a higher value indicates fewer large events and more small events than a lower value.

We estimate b -values via nonlinear parameter fitting for the parameters c and b over a specific magnitude range (M_c , M_{max}), assuming a magnitude-bounded Gutenberg–Richter law formulated as

$$N = c 10^{-bM} (M_c \leq M \leq M_{\text{max}}). \quad (3)$$

The magnitude range was dynamically specified for each sample population of earthquakes. The minimum magnitude value M_c was estimated using the maximum curvature approach of Wiemer and Wyss (2000). To combat the issue of underestimation of M_c in the case of gradually curved FMDs (Woessner and Wiemer, 2005) and to ensure catalog completeness, M_c was reset to include only the upper 85% of the magnitude range beyond the M_c estimated using maximum

curvature. The maximum magnitude was the maximum magnitude event in each population. The magnitudes of each sample population were used to estimate a probability density function (PDF) with standard errors (Brandon, 1996). A weighted least-squares nonlinear parameter estimation of c and b was then fit to the PDF estimate using a grid search, followed by refinement using the Levenberg–Marquardt method (e.g., Aster *et al.*, 2013). The covariance matrix of the parameters was then calculated from the Jacobian of the weighted least-squares minimization function. Synthetic catalogs drawn from the Gutenberg–Richter law (equation 2) were generated to confirm that 95% confidence intervals on b estimated from the covariance matrix model were accurate for a range of synthetic catalog M and b -values, as well as magnitude-axis discretization. A p -value test was performed for each parameter determination to ensure χ^2 -consistent adherence between parameter-predicted and empirical PDFs.

RESULTS

Subspace detectors were used to detect recent earthquakes near Guthrie, Oklahoma, using the two closest seismic stations (GS.OK029 and GS.OK027). From empirical analysis of the observed waveforms recorded on station GS.OK029, a 4–16 Hz filter band was found to capture signals for the broadest range of earthquake magnitudes. For frequencies below ~ 4 Hz, smaller events could be filtered out, whereas above 16 Hz there was no improvement in the signal-to-noise ratio. For the 79 earthquakes used to determine an optimal set of subspace detectors, the waveforms were bandpass filtered on all three broadband channels, and each of them was aligned via cross correlation on the largest amplitude phase (S wave) observed on the horizontal components. A 1.4 s window starting 1.3 s before the onset of the direct S -wave arrival then was selected. The 1.4 s window of data includes both the P and complete S wave observed at the station. The singular value decomposition of the 79 three-component waveforms results in seven multichannel templates (orthonormal basis functions) that describe 90% of the observed event waveform data (Fig. 2b).

The templates are characterized by relatively low-amplitude P -wave phases (nodal, based on source mechanisms) and distinct S -wave phases on both horizontal components, making the signal generally unique. It is important to note that three-component processing is important in Oklahoma, where almost all observed earthquakes are relatively shallow and have predominantly strike-slip mechanisms of similar orientation (McNamara *et al.*, 2015). Consequently, waveforms across the region can look similar, with relatively simple and strong S -wave pulses. Using a waveform that includes the nodal P -wave phase thus becomes an important constraint. Other source regions may have similar-looking S -wave pulses, but differences in the P -wave amplitudes and phase delays between the P - and S -wave pulses minimize detections of earthquakes from other source regions.

A 1.4-s-long multichannel template is the shortest template that contains the full P - and S -wave pulses in these data. This relatively short template length can increase the chance of false detections; however, we compensated for this using a high-detection threshold (6σ). In addition, we also re-performed the analysis using template lengths of 2.0 and 3.0 s, which include a significantly longer portion of the S coda. These longer templates produced results that were highly similar to those of the 1.4-s template length.

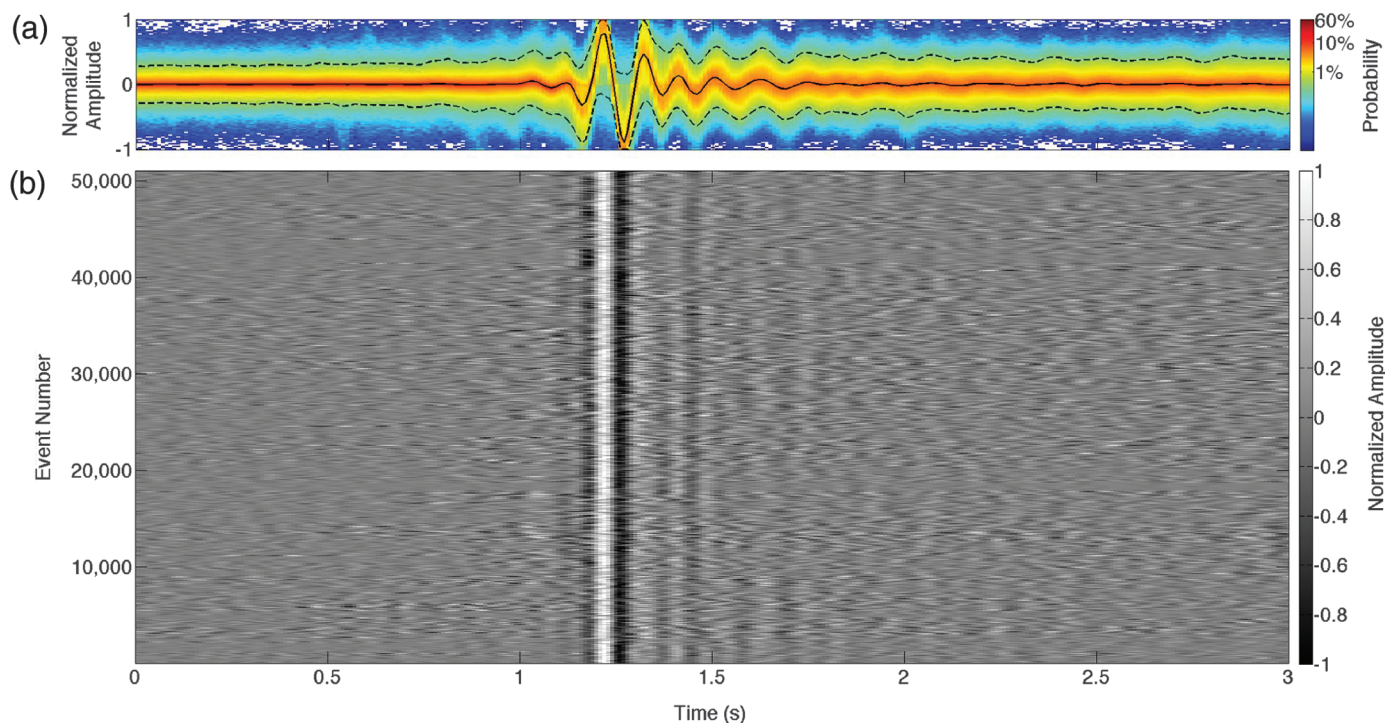
For the Guthrie cluster, variability in the observed waveforms is primarily associated with changes in source depth. Shallow earthquakes exhibit stronger dispersion of the surface waves due to the shallow low-velocity structure, whereas deeper earthquakes are typically characterized by relatively simple horizontal-component waveforms. The subspace templates also show polarity differences in the S wave that are likely related to changes in source mechanism or changes in spatial location along the fault zone.

Continuous correlation of the optimal detectors with station GS.OK029 from 15 February 2014 through 31 August 2014 resulted in 51,112 detections (Fig. 3) and a minimum magnitude of completeness of 0.1. A maximum number of detections per day of 2462 occurred on 17 February 2014, whereas the fewest number of earthquakes was 84 on 19 June 2014. The average number of detections per day was 258. None of the detected earthquakes are associated with previously reported earthquakes in other parts of Oklahoma.

All the detected waveforms recorded on the HH1 component (north–south-oriented channel) for station GS.OK029 are shown as a PDF (Fig. 3a) and as aligned normalized traces (Fig. 3b). The PDF was computed by stacking and binning trace-normalized waveforms on a point-by-point basis. Both figures show the remarkable similarity of the waveforms. The PDF also highlights that the highest probabilities are consistent with the highest-ranking templates (Fig. 2) and that low probabilities (less than a few percent) are primarily related to low signal-to-noise detections. The lack of significant variability in the templates indicates a relatively small active faulting region.

A summary of the detections with time (Fig. 4) shows that peaks in the number of detections per day generally associate with the occurrence of larger earthquakes ($M > 3.0$). Each peak in the seismicity rate exhibits two common features: (1) an increase in the number of earthquakes per day preceding the peak and (2) a rapid decay in the number of earthquakes occurring over several days following the peak. Although tectonic sequences generally follow an Omori-type exponential decay law (Ishimoto and Iida, 1939; Gutenberg and Richter, 1944) to a background rate, the Guthrie earthquakes decay only to a generally high-sustained rate of several hundred earthquakes per day with episodic pulses to higher rates.

Using the same processing procedures for the next closest station, GS.OK027, which is 16.5 km from the centroid of the earthquake cluster, we noted $\sim 15\%$ of the earthquakes detected on GS.OK029 with a minimum magnitude of completeness of 0.2 (see $\text{\textcircled{E}}$ Fig. S3, available in the electronic supplement of this article). The temporal variations in b -value for station



▲ **Figure 3.** All detected waveforms observed on the horizontal channel HH1 (component oriented north–south) for station GS.OK029: (a) the probability density function stack was computed by trace-normalizing the detection waveforms and binning them as a probability on a point-by-point basis. The solid black line shows the median waveform, and the dashed lines show the $\pm 3\sigma$ envelope of the distribution. (b) Aligned waveforms of all 51,112 detections shaded by normalized amplitude.

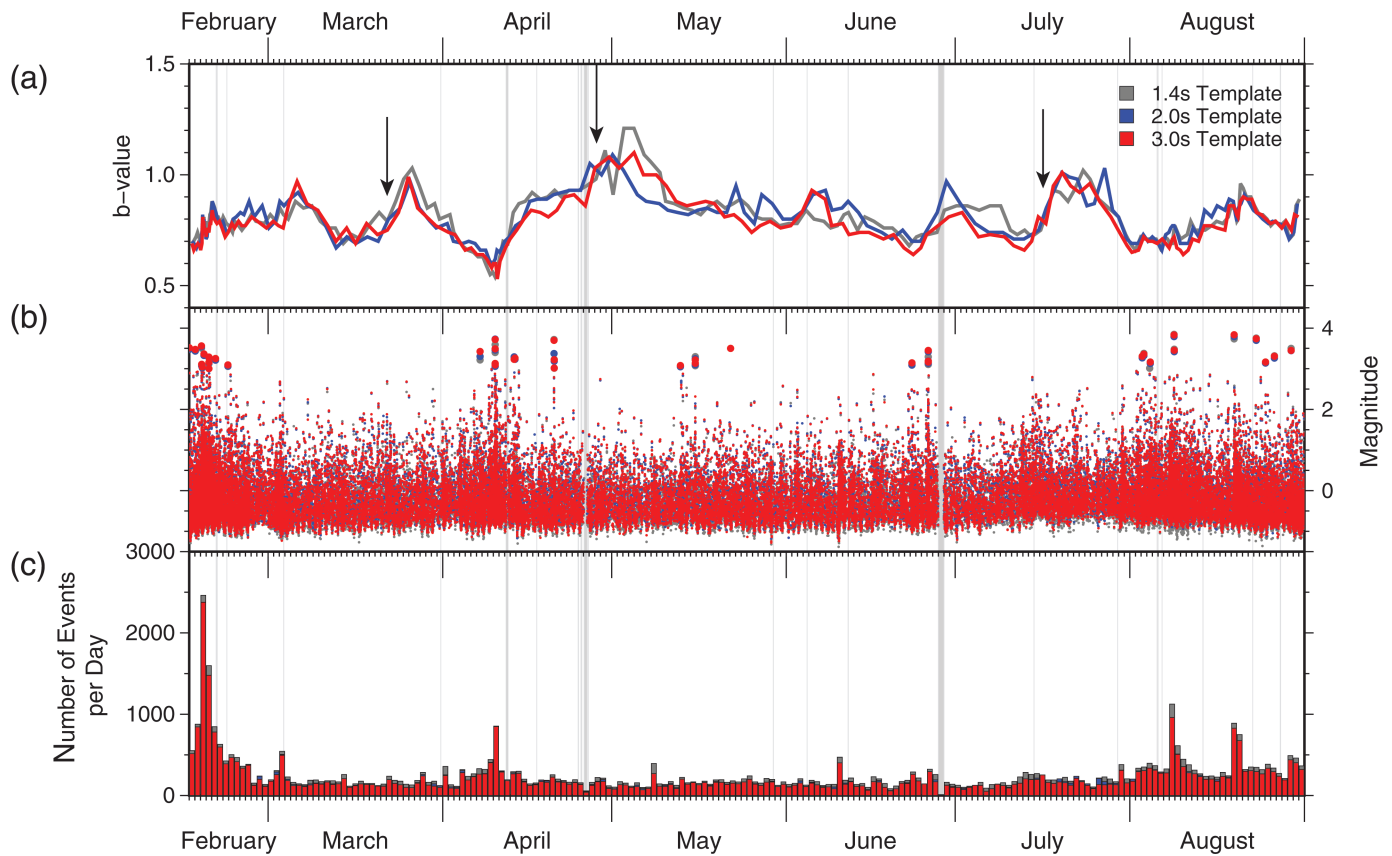
GS.OK027 are consistent with those observed for station GS.OK029.

A complication in the modeling of this earthquake sequence is the emergence of an earthquake cluster northeast of station GS.OK029 (Fig. 1), first documented by the occurrence of a 14 July 2014 *M* 2.5 event. The two earthquake sequences are spatially close and roughly equidistant to stations GS.OK027 and GS.OK029. Both sequences are also characterized by shallow seismicity and similar source mechanisms. Regional moment tensor solutions for events in the two clusters reveal two subparallel strike-slip faults oriented northeast–southwest (Fig. 1). Station GS.OK029 lies in the same part of the focal sphere for each cluster but on the opposite side of the mechanism. Consequently, subspace detectors constructed from earthquakes in the southwest cluster are likely to detect earthquakes in the northeast cluster. Using longer templates that included more of the coda was not diagnostic enough to significantly eliminate events in this second cluster. Separating the two clusters to very small magnitudes would require additional close stations that are not equidistant to the clusters. Data for the next closest stations were too intermittent to help identify when the northeast sequence began. We assume that prior to 1 June 2014 our detection results are dominated by activity within the southwest cluster, whereas after 1 June 2014 the results are a mix of activity from the two clusters.

Several studies (Wiemer and Wyss, 2000; Schorlemmer *et al.*, 2005; Farrell *et al.*, 2009; Bachman *et al.*, 2012) used

b-value as a diagnostic indicator of seismogenic variability mechanisms that include changes in stress and/or thermal conditions, the presence of fluids, and variations in source zone constitutive properties (e.g., highly fractured versus competent rock). A global study of *b*-value (Schorlemmer *et al.*, 2005) shows that areas of active tectonics generally exhibit a value near 1.0, whereas volcanic systems and induced-seismicity sequences are generally characterized by a *b*-value greater than 1.0. Earthquake sequences or regions characterized by high *b*-values are attributed to increased pore pressure from fluid migration or injection (i.e., magmatic or hydrothermal fluids or wastewater) that leads to fault weakening and associated increases in seismicity (Farrell *et al.*, 2009; Bachman *et al.*, 2012).

The large number of earthquakes recorded per day combined with estimates of magnitude allows us to compute varying *b*-values for the sequence at high temporal resolution. Our *b*-value results show variations that range from as low as 0.5 to as high as 1.2, with an average *b*-value of 0.80 (Fig. 4). The calculated *b*-value for the catalog as a whole is 0.82 (see Fig. S1). Friberg *et al.* (2014) suggest, in relation to hydraulic fracturing sequences, that higher *b*-values are associated with microearthquakes generated from the creation of new fractures, whereas lower *b*-values are associated with reactivation of pre-existing faults. In the Guthrie sequence, we believe earthquakes are occurring along a preexisting fault in the shallow portion of the crystalline basement. We observed a sharp positive *b*-value



▲ **Figure 4.** Detector summary as a function of time for data from station GS.OK029. All three figures display results using template lengths of 1.4 s (dark gray), 2.0 s (blue), and 3.0 s (red). (a) The time-varying b -value is estimated using a sliding window of 500 earthquakes; (b) detection magnitudes, larger dots indicating events larger than M 3.0; and (c) number of detections per day. The light gray vertical lines show time periods without data. The black arrows indicate the sharp positive b -value gradients that preceded larger earthquakes (M 3 or larger). The b -value decreases as the processing window encompasses the larger earthquakes and trends toward the background rate as the larger earthquakes slide out of the window. Note that all three template lengths show similar detection numbers, magnitudes, and b -value trends, indicating that results are not strongly affected by template length.

gradient over approximately a few days to one week preceding the largest observed earthquakes, typically one magnitude unit larger than background levels. When the processing window encompasses the largest earthquake swarms, characterized by increased numbers of events per day and magnitude, b -value sharply drops for a few days. Following these larger earthquake swarms, b -values trend gradually upward. These results suggest that variations in b -value are a direct measure of the changes of stress to the fault systems. If the subspace detector fails to detect events outside the predefined cluster, the trends seen before and after larger earthquakes will likely not change.

In the absence of information on the wastewater injection volumes and rates at the nearby disposal wells, we must speculate on the details of how injected wastewater may act to weaken faults via an increase in pore pressure. The results here show that the Guthrie sequence is atypical of tectonically controlled earthquake sequences where one would expect the rate and magnitude of earthquakes to decline with time after larger events. High sustained rates of seismicity and highly variable

b -values over short time durations suggest that wastewater injection is a contributing factor in controlling the sustained seismicity in this area; and, as such, we can construct a hypothesis to explain our observations.

Our observations of progressive time-varying b -value variations suggest that fluid migration in the fault zone decreases the fault-normal stresses (i.e., increasing the seismogenic potential of the deviatoric stresses) on the fault (Raleigh *et al.*, 1976; Nicholson and Wesson, 1990). This weakening process manifests itself as an increase in small earthquakes (higher b -value). This process continues to the point of critical failure where a larger patch of the fault system is able to slip in a series of larger earthquakes ($M > 3$). The larger earthquakes effectively strengthen the fault by eliminating the fluid pathways, resulting in a resetting of the system to higher normal stresses that inhibit earthquakes. The cycle repeats itself as migrating fluids reestablish pathways along the fault system and again decrease effective stress. For this to be sustained, the associated cumulative stress drops must be partial (significantly less than the

available deviatoric stress) so that deviatoric stress remains to drive ongoing activity.

This article documents a novel approach for detailed characterization of spatiotemporal variations in clustered seismicity using a single station. The FMDs in seismicity are easily quantified from time-varying estimates of b -value, variations of which provide insight into possible mechanisms for earthquake generation in the presence of fluids.

CONCLUSION

This study demonstrates that an optimal set of subspace detectors is effective at targeting and characterizing occurrence and magnitude of earthquake sequences of interest and, when combined with observations of time-varying b -values, provides possible insight into time-varying fault behavior and seismicity forecasting. The USGS catalog of earthquake source parameters for Oklahoma is sufficient to design optimal sets of waveform templates, both retrospectively and in real time, which can vastly improve monitoring of numerous earthquake sequences that have developed throughout Oklahoma in recent years (McNamara *et al.*, 2015).

DATA AND RESOURCES

The waveform data used in this study can be obtained from the Incorporated Research Institutions for Seismology (IRIS) Data Management Center (<http://www.iris.edu/>; last accessed December 2015). Earthquake source parameters and phase data used to construct optimal waveform templates were obtained from U.S. Geological Survey recent earthquake web pages (<http://earthquake.usgs.gov/earthquake/search/>; last accessed December 2014). © Estimated origin times and magnitudes for detected earthquakes in this study can be found in the electronic supplement (see Table S1). Class II injection well information was obtained from the Oklahoma Corporation Commission electronic well database (<http://www.occperrmit.com/WellBrowse/>; last accessed May 2015) and oil and gas data files (<http://www.occeweb.com/og/ogdatafiles2.htm>; last accessed May 2015). Some figures were created using the Generic Mapping Tools software of Wessel *et al.* (2013). ✉

ACKNOWLEDGMENTS

This research was supported by the U.S. Geological Survey (USGS) National Earthquake Hazards Reduction Program. Kevin Furlong, Paul Earle, Rob Williams, and Oliver Boyd of the USGS, Michael Brudzinski, and two anonymous reviewers provided thoughtful comments that improved this article. We thank N. Vance and J. McCarthy for editorial reviews. The authors greatly appreciate the hard work of the people who responded to the evolving earthquake sequence. Any use of trade, product, or firm names is for descriptive purposes only and does not imply endorsement by the U.S. Government.

REFERENCES

- Aster, R., B. Borchers, and C. Thurber (2013). *Parameter Estimation and Inverse Problems*, Elsevier, Amsterdam, The Netherlands, 360 pp.
- Bachman, C. E., S. Wiemer, B. P. Goertz-Allmann, and J. Woessner (2012). Influence of pore-pressure on the event-size distribution of induced earthquake, *Geophys. Res. Lett.* **39**, L09302, doi: [10.1029/2012GL051480](https://doi.org/10.1029/2012GL051480).
- Brandon, M. (1996). Probability density plot for fission-track grain-age samples, *Radiat. Meas.* **26**, 663–676.
- Ellsworth, W. L. (2013). Injection-induced earthquakes, *Science* **341**, doi: [10.1126/science.1225942](https://doi.org/10.1126/science.1225942).
- Farrell, J., S. Husen, and R. B. Smith (2009). Earthquake swarm and b -value characterization of the Yellowstone volcanic-tectonic system, *J. Volcanol. Geotherm. Res.* **188**, 260–276.
- Friberg, P. A., G. M. Besana-Ostman, and I. Dricker (2014). Characterization of an earthquake sequence triggered by hydraulic fracturing in Harrison County, Ohio, *Seismol. Res. Lett.* **85**, 1295–1307.
- Gutenberg, B., and C. F. Richter (1944). Frequency of earthquakes in California, *Bull. Seismol. Soc. Am.* **34**, 185–188.
- Harris, D. B. (2006). Subspace detector: Theory, *Lawrence Livermore National Laboratory UCRL-TR-222758*, 1–48.
- Harris, D. B., and D. A. Dodge (2011). An autonomous system for grouping events in a developing aftershock sequence, *Bull. Seismol. Soc. Am.* **101**, 763–774, doi: [10.1785/0120100103](https://doi.org/10.1785/0120100103).
- Herrmann, R. B., H. Benz, and C. J. Ammon (2011). Monitoring the earthquake source process in North America, *Bull. Seismol. Soc. Am.* **101**, 2609–2625, doi: [10.1785/0120110095](https://doi.org/10.1785/0120110095).
- Holland, A. A. (2013). Optimal fault orientation within Oklahoma, *Seismol. Res. Lett.* **84**, 876–890, doi: [10.1785/0220120153](https://doi.org/10.1785/0220120153).
- Ishimoto, M., and K. Iida (1939). Observations sur les seisms euegreste par le microseisograph construite dernièrement (I), *Bull. Earthq. Res. Inst.* **17**, 443–478 (in French).
- Kim, W. (2013). Induced seismicity associated with fluid injection into a deep well in Youngstown, Ohio, *J. Geophys. Res.* **118**, 3506–3518.
- McNamara, D. E., H. M. Benz, R. B. Herrmann, E. A. Bergman, P. Earle, A. Holland, R. Baldwin, and A. Gassner (2015). Earthquake hypocenters and focal mechanisms in central Oklahoma reveal a complex system of reactivated subsurface strike-slip faulting, *Geophys. Res. Lett.* **42**, doi: [10.1002/2014GL062730](https://doi.org/10.1002/2014GL062730).
- Nicholson, C., and R. L. Wesson (1990). Earthquake hazard associated with deep well injection: A report to the U.S. Environmental Protection Agency, *U.S. Geol. Surv. Bull.* 1951, <http://pubs.usgs.gov/bul/1951/report.pdf> (last accessed May 2015).
- Raleigh, C. B., J. H. Healy, and J. D. Bredehoeft (1976). An experiment in earthquake control at Rangely, Colorado, *Science* **191**, 1230–1237, doi: [10.1126/science.191.4233.1230](https://doi.org/10.1126/science.191.4233.1230).
- Schorlemmer, D., S. Wiemer, and M. Wyss (2005). Variations in earthquake-size distribution across different stress regimes, *Nature* **437**, 539–542.
- Skomal, R. J., M. R. Brudzinski, B. S. Currie, and J. Levy (2014). Optimizing multi-station earthquake template matching through re-examination of the Youngstown, Ohio sequence, *Earth Planet. Sci. Lett.* **405**, 274–280.
- Wessel, P., W. H. F. Smith, R. Scharroo, J. Luis, and F. Wobbe (2013). Generic Mapping Tools: Improved version released, *Eos Trans. AGU* **94**, no. 45, 409–410, doi: [10.1002/2013EO450001](https://doi.org/10.1002/2013EO450001).
- Wiemer, S., and M. Wyss (2000). Minimum magnitude of complete reporting in earthquake catalogs: Examples from Alaska, the western United States, and Japan, *Bull. Seismol. Soc. Am.* **90**, 859–869.
- Woessner, J., and S. Wiemer (2005). Assessing the quality of earthquake catalogs: Estimating the magnitude of completeness and its uncertainty, *Bull. Seismol. Soc. Am.* **95**, 684–698.

*Harley M. Benz
Nicole D. McMahon
Daniel E. McNamara
National Earthquake Information Center
U.S. Geological Survey
Denver Federal Center
Box 25046, MS 966
Denver, Colorado 80225 U.S.A.
benz@usgs.gov
nmcMahon@usgs.gov
mcnamara@usgs.gov*

*Richard C. Aster
Department of Geosciences
Colorado State University
Fort Collins, Colorado 80523 U.S.A.
Rick.Aster@colostate.edu*

*David B. Harris
Deschutes Signal Processing
81211 East Wapinitia Road
Maupin, Oregon 97037 U.S.A.
oregondsp@gmail.com*